

Optical Investigation of Broadband White-Light Emission in Self-Assembled Organic-Inorganic Perovskite (CHNH)PbBr

Aymen Yangui, Damien Garrot, Jean-Sébastien Lauret, Alain Lusson, Guillaume Bouchez, Emmanuelle Deleporte, Sebastien Pillet, El-Eulmi Bendeif, Miguel Castro, Smail Triki, Younes Abid, and Kamel Boukheddaden

J. Phys. Chem. C, **Just Accepted Manuscript** • DOI: 10.1021/acs.jpcc.5b06211 • Publication Date (Web): 11 Sep 2015

Downloaded from <http://pubs.acs.org> on September 15, 2015

Just Accepted

“Just Accepted” manuscripts have been peer-reviewed and accepted for publication. They are posted online prior to technical editing, formatting for publication and author proofing. The American Chemical Society provides “Just Accepted” as a free service to the research community to expedite the dissemination of scientific material as soon as possible after acceptance. “Just Accepted” manuscripts appear in full in PDF format accompanied by an HTML abstract. “Just Accepted” manuscripts have been fully peer reviewed, but should not be considered the official version of record. They are accessible to all readers and citable by the Digital Object Identifier (DOI®). “Just Accepted” is an optional service offered to authors. Therefore, the “Just Accepted” Web site may not include all articles that will be published in the journal. After a manuscript is technically edited and formatted, it will be removed from the “Just Accepted” Web site and published as an ASAP article. Note that technical editing may introduce minor changes to the manuscript text and/or graphics which could affect content, and all legal disclaimers and ethical guidelines that apply to the journal pertain. ACS cannot be held responsible for errors or consequences arising from the use of information contained in these “Just Accepted” manuscripts.

1
2
3
4
5
6
7
8
9
10
11
12
13
14
15
16
17
18
19
20
21
22
23
24
25
26
27
28
29
30
31
32
33
34
35
36
37
38
39
40
41
42
43
44
45
46
47
48
49
50
51
52
53
54
55
56
57
58
59
60

Optical Investigation of Broadband White-Light Emission in Self-Assembled Organic-Inorganic Perovskite (C₆H₁₁NH₃)₂PbBr₄

A. Yangui,^{a,b} D. Garrot,^{a*} J.S. Lauret,^c A. Lussion,^a, G. Bouchez^a, E. Deleporte,^c S. Pillet,^d E.E Bendeif,^d M. Castro,^e S. Triki,^f Y. Abid^b and K. Boukheddaden^{a*}

^a Groupe d'Etudes de la Matière Condensée (GEMaC), CNRS, Université de Versailles Saint-Quentin-en-Yvelines, 45 Avenue des Etats-Unis 78035 Versailles cedex, France

^b Laboratoire de Physique Appliquée (LPA), Faculté des Sciences de Sfax, Route de Soukra km 3.5 BP 1171, 3018 Sfax, Tunisie

^c Laboratoire Aimé Cotton, Ecole Normale Supérieure de Cachan, CNRS, Université de Paris-Sud, Bât 505 Campus d'Orsay, 91405 Orsay, France

^d Université de Lorraine, CRM2, UMR 7036, Vandoeuvre-les-Nancy, F-54506, France,

^e Instituto de Ciencia de Materiales de Aragón (CSIC-Universidad de Zaragoza), Departamento de Ciencia y Tecnología de Materiales y Fluidos, Escuela de Ingeniería y Arquitectura, C/ Maria de Luna nº3, 500018 Zaragoza, Spain

^f Laboratoire de Chimie, Electrochimie Moléculaires et Chimie Analytique, CNRS, Université de Bretagne Occidentale, BP 809, 29285 Brest, France

AUTHOR INFORMATION

*Corresponding Authors: damien.garrot@uvsq.fr, kbo@physique.uvsq.fr

1
2
3
4
5
6
7
8
9
10
11 **ABSTRACT.** The performance of hybrid organic perovskite (HOP) for solar energy conversion
12 is driving a renewed interest in their light emitting properties. The recent observation of broad
13 visible emission in layered HOP highlights their potential as white light emitters. Improvement of
14 the efficiency of the material requires a better understanding of its photophysical properties. We
15 present in-depth experimental investigations of white light (WL) emission in thin films of the
16 $(\text{C}_6\text{H}_{11}\text{NH}_3)\text{PbBr}_4$. The broadband, strongly Stokes shifted emission presents a maximum at 90K
17 when excited at 3.815 eV, and below this temperature coexists with an excitonic edge emission.
18 X-rays and calorimetry measurements excludes the existence of a phase transition as an origin of
19 the thermal behavior of the WL luminescence. The free excitonic emission quenches at low
20 temperature, despite a binding energy estimated to 280 meV. Time-Resolved Photoluminescence
21 spectroscopy reveals the multicomponent nature of the broad emission. We analyzed the
22 dependence of these components as function of temperature and excitation energy. The results are
23 consistent with the existence of self-trapped states. The quenching of the free exciton and the
24 thermal evolution of the WL luminescence decay time are explained by the existence of an energy
25 barrier against self-trapping, estimated to ~ 10 meV.
26
27
28
29
30
31
32
33
34
35
36
37
38
39
40
41
42
43
44
45
46
47
48
49
50
51

52 **I. INTRODUCTION**

53
54

55 During the last decades, a great attention has been devoted to the large family of hybrid organic
56 perovskites (HOP) due to their special structural features and their important optical properties.
57
58
59
60

1
2
3 These materials are known to crystallize in zero-, one-, two or three dimensional structures.^{1,2} The
4
5 3D HOP have drawn considerable attention since 2012 for their application in photovoltaic
6
7 devices.³⁻⁶ In particular, $(\text{CH}_3\text{NH}_3)\text{PbI}_3$ and its derivatives present exceptional potential for the
8
9 fabrication of hybrid solar cells with efficiencies approaching 20%.⁷ Recently, amplified
10
11 spontaneous emission has also been reported, which makes these materials attractive candidates
12
13 for the realization of on-chip coherent light source.⁸ Their 2D counterpart have the general
14
15 chemical formula $(\text{R-NH}_3)_2\text{MX}_4$ or $(\text{H}_3\text{N-R-NH}_3)\text{MX}_4$, where R is an organic group, M a divalent
16
17 metal and X a halogen. They can be easily deposited as thin films by the spin coating technique
18
19 and self-assembled in a multi-quantum well structure.^{1,9} The carriers are confined in the inorganic
20
21 part formed by MX_6^{2-} octahedra and the organic part acts like a potential barrier (Figure 1).
22
23 Besides, the high dielectric contrast between the organic and inorganic part contributes to
24
25 strengthen the 2D confinement by image charge effect.¹⁰ These mechanisms lead to the existence
26
27 of excitons with large binding energy of a few hundred of meV.^{11,12} 2D HOP exhibit strong
28
29 photoluminescence¹² and electroluminescence¹³⁻¹⁵, even at room temperature, which makes them
30
31 legitimate candidates for an integration in electronic and optoelectronic devices such as organic -
32
33 inorganic light emitting diodes (OILED), field effect transistors, or polariton lasers.^{12,13,15-17} In
34
35 addition, the electronic and optical properties of 2D HOP can be controlled through chemical
36
37 engineering of the organic part.¹⁸⁻²⁰ On contrary, the choice of the organic part for 3D HOP is
38
39 limited because the molecule has to be small enough to maintain the 3D structure.
40
41
42
43
44
45
46
47

48 Very recently, Dohner and al.^{21,22} have observed white light emission under UV irradiation in
49
50 two families of hybrid perovskites, namely $(\text{N-MEDA})\text{PbBr}_{4-x}\text{Cl}_x$ (N-MEDA=N¹-methyl-ethane-
51
52 1,2-diammonium) and $(\text{EDBE})\text{PbBr}_4$ (EDBE = 2,2'-(ethylenedioxy)bis(ethylammonium)) with X
53
54 = Cl or Br. The chromaticity of the emission was partially tuned with the choice of the halogen
55
56
57
58
59
60

1
2
3 and a stable Photoluminescence Quantum Efficiency (PLQE) of 9% has been measured. These
4
5 results highlight the great potential of these materials as white light emitters.
6
7

8 However, the physical origin of this phenomenon is still uncertain. A better understanding of its
9
10 photophysical properties and the possibility of chemical engineering should lead to the design of
11
12 material with improved PLQE. We report here on the optical properties of a broad white light
13
14 emission in the 2D HOP (C₆H₁₁NH₃)₂PbBr₄, under UV irradiation. The manuscript is organized
15
16 as follows: Sec. II details the experimental methods used in the present study; Sec. III is devoted
17
18 to the experimental results and their interpretation, and in Sec. IV, we conclude.
19
20
21
22
23

24 II. EXPERIMENTAL METHODS

25
26
27
28 **Synthesis** All reagents were purchased from commercial vendors and used as received. The
29
30 purity of the products used is greater than 99%. Solvents were of reagent grade or higher purity.
31
32 All manipulations were conducted in air. In a first step, the ammonium salt C₆H₁₁NH₃⁺Br⁻ was
33
34 prepared using the reaction between cyclohexylamine (C₆H₁₁NH₂) and HBr (47 wt %) to a cold (-
35
36 20°C), in order to remove the reaction heat, with stirring for 20 minutes. Water was evaporated by
37
38 elevating the temperature followed by washing with diethyl ether. The colorless precipitate was
39
40 dried under vacuum in order to obtain a very clean product. In a second step, a 367 mg of PbBr₂
41
42 (1 mmol) in 2-ml of HBr (47 wt %) was added to 360 mg of C₆H₁₁NH₃⁺Br⁻ and mixed in the
43
44 methanol solvent, at room temperature. After 3 days, colorless platelets were formed. The purity
45
46 of solution was improved by second re-crystallization.
47
48
49
50

51
52 **Crystal structure.** Colorless single crystal of (C₆H₁₁NH₃)₂PbBr₄ with approximate dimensions
53
54 0.08×0.27×0.32 mm³ was selected for the x-ray diffraction experiments. The X-ray data collection
55
56 was carried out using a supernova 4-circle micro-source diffractometer (Oxford Diffraction)
57
58
59
60

1
2
3 equipped with a two-dimensional ATLAS detector, and using graphite monochromatized Mo K α
4 radiation ($\lambda = 0.71073 \text{ \AA}$). Data were collected at 293 K. The structure was solved by direct
5 methods and successive Fourier difference syntheses, and was refined on F^2 by weighted
6 anisotropic full-matrix least-square methods using SHELX-2013 crystallographic software
7 package.²³ All non-hydrogen atoms were refined anisotropically while the hydrogen atom were
8 calculated and therefore included as isotropic fixed contributors to F_C . Data collection and data
9 reduction were carried out using the CRYALIS-CCD and CRYALIS-RED programs²⁴.

10
11
12
13
14
15
16
17
18
19
20 Single crystal X-ray studies were collected at $T = 20\text{K}$, 50K and 90K on a Microfocus Supernova
21 diffractometer equipped with a two dimensional ATLAS detector, using Mo K α radiation ($\lambda =$
22 0.71073 \AA), and a Helijet He open flow cryosystem. Numerical absorption correction was
23 performed according to the crystal faces. The corresponding structures were solved by direct
24 methods with the SHELXS program and refined on F^2 by weighted full matrix least-squares
25 methods using the SHELXL program. All non-hydrogen atoms were refined anisotropically,
26 hydrogen atoms were generated at their ideal positions and treated using a riding model. The
27 ammonium cation exhibits severe disorder which was treated using two configurations whose
28 population P1 and P2 was refined with the constraint $P1+P2=1.0$. The disordered non hydrogen
29 atoms of the ammonium cation was restricted to isotropic atomic displacement parameters and
30 constrained to be equivalent for the two cation orientations.
31
32
33
34
35
36
37
38
39
40
41
42
43
44
45
46
47

48 **Films** Thin film of $(\text{C}_6\text{H}_{11}\text{NH}_3)_2\text{PbBr}_4$ was prepared by spin coating technique. The thickness was
49 estimated to 300 nm with surface profilometry. 20 mg of $(\text{C}_6\text{H}_{11}\text{NH}_3)_2\text{PbBr}_4$ crystal was dissolved
50 in 1.1 ml of N-N-dimethylformamide (DMF) solvent and spin-coated on a quartz slides at 1500
51 rpm for 20 s. The film was then annealed at 80°C for 30 min to remove residual solvent.
52
53
54
55
56
57
58
59
60

1
2
3
4
5
6 **Calorimetry** Heat capacity was determined in the temperature range of 25-200 K by thermal
7
8 relaxation calorimetry using the Quantum Design's Physical Property Measurement System
9
10 (PPMS). A few small crystals of $(\text{C}_6\text{H}_{11}\text{NH}_3)\text{PbBr}_4$, with a total mass of around 1 mg, were
11
12 mounted pressing them over a small amount of Apiezon N Grease applied as a layer onto the
13
14 sample platform. The reported heat capacity data, after subtracting the contribution of the sample
15
16 platform, corresponds to the heat capacity of both the crystals and Apiezon N Grease.
17
18 Approximately, the sample contributes to around 40 % and 7% of the total measured heat capacity
19
20 (sample platform+ Apiezon N grease + sample) at 20 K and 180 K respectively.
21
22
23
24
25
26

27 **Optical measurements** Absorption measurements were taken on spin-coated film and deduced
28
29 from direct transmission measurements performed using a conventional UV-visible
30
31 spectrophotometer (HITACHI, U-3300). For the PLE measurement, the excitation source was a
32
33 Xenon arc lamp filtered with a monochromator. The photoluminescence spectra were recorded
34
35 using a spectrapro 2500i spectrometer equipped with a Pixis: 100B CCD array detector (Ropers
36
37 scientific). The excitation wavelength was the 325 nm (3.815 eV) line of a He-Cd laser. The sample
38
39 was placed on the cold finger of a helium closed cycle cryostat. Time-resolved photoluminescence
40
41 were performed using the Time-Correlated Single Photon Counting TimeHarp 260 system from
42
43 PicoQuant. The excitation was the second harmonic of a pulse from a Ti:Sapphire laser (Mai Tai,
44
45 Spectra-Physics). The emission was detected with a single photon avalanche diode (IDQuantique
46
47 ID150). Repetition rate was adjusted thanks to a pulse picker (Spectra Physics) from 80MHz to
48
49 80 kHz.
50
51
52
53
54
55
56
57
58
59
60

Table 1. Crystallographic data for $(C_6H_{11}NH_3)_2PbBr_4$

Empirical Formula	$C_{12}H_{28}Br_4N_2Pb$
Temperature, K	293
Formula weight, $g \cdot mol^{-1}$	711.1
Wavelength, \AA	Mo $K\alpha$ ($\lambda = 0.71073 \text{\AA}$)
Crystal system	Orthorhombic
Space group	$Cmc2_1$
a , \AA	27.7311(11)
b , \AA	8.6525(3)
c , \AA	8.2029(4)
Volume, \AA^3	1968.23
Z	4
Density (calculated), $g \cdot cm^{-3}$	2.40
Absorption coefficient, mm^{-1}	16.682
$F(000)$	1280
Crystal size, mm^3	0.08 x 0.27 x 0.32
Crystal color/shape	Colorless/Platelets
Maximum 2θ , deg	63.05
hkl range	$h = -40/40, k = -12/12, l = -11/7$
Reflexions collected/unique	16235/2300
Data with $F_0 > 4\sigma(F_0)$	2051
Highest peak/deepest hole, $e \cdot \text{\AA}^{-3}$	5.22/-2.78
Goodness-of-fit	1.064
R_{int}	0.0419
R (sigma)	0.0372
wR_2^a	0.1231
R_1^b (obs data) / R_1 (all data)	0.0462 / 0.055

$${}^a wR_2 = \left[\frac{\sum w(F_0^2 - F_c^2)^2}{\sum F_0^2} \right]^{1/2}, {}^b R_1 = \frac{\sum ||F_0| - |F_c||}{\sum |F_0|}$$

III. RESULTS AND DISCUSSION

(C₆H₁₁NH₃)₂PbBr₄ crystallizes in the orthorhombic system Cmc2₁ space group, with a primitive unit cell of dimensions: *a* = 27.7311 Å, *b* = 8.6525 Å, *c* = 8.2029 Å and four formula units (*Z* = 4), at room temperature. The relevant structural data are summarized in Table 1. Crystal structure shows a two-dimensional (2D) periodic arrangement of the inorganic layers formed by corner-sharing PbBr₆ octahedra and the organic layers C₆H₁₁NH₃⁺ (Figure 1). The organic sheets of layered perovskites can be derived from the (100) crystallographic planes of the three-dimensional perovskite structure.

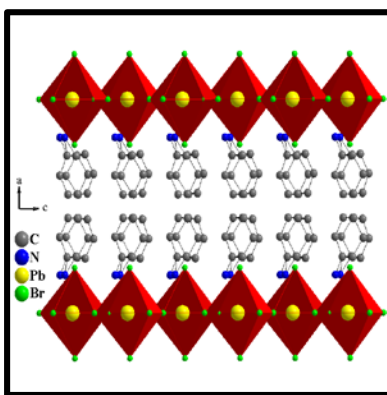


Figure 1. Sketch of the X-ray diffraction structure of (C₆H₁₁NH₃)₂PbBr₄ single crystal.

Absorption spectrum of spin-coated thin film of (C₆H₁₁NH₃)₂PbBr₄ (Figure 2a) shows a similar behavior to those of other lead bromide hybrid perovskites^{20,25–28} with a sharp excitonic absorption peaked at 3.19 eV and an absorption continuum at higher energy. The absorption band at 3.85 eV has been ascribed to inter-band transition.¹² Upon 325 nm (3.815 eV) excitation,

(C₆H₁₁NH₃)₂PbBr₄ shows a very broad emission, structureless and Gaussian shaped, with a large Stokes shift (1.2 eV) that spans the entire visible spectrum, with a maximum intensity at 2 eV and a full width at half maximum (FWHM) of 660 meV (Figure 2b). The excitation spectra (PLE) recorded with a detection energy of 2 eV coincides with the excitonic and the absorption continuum of the perovskite (Figure 2b).

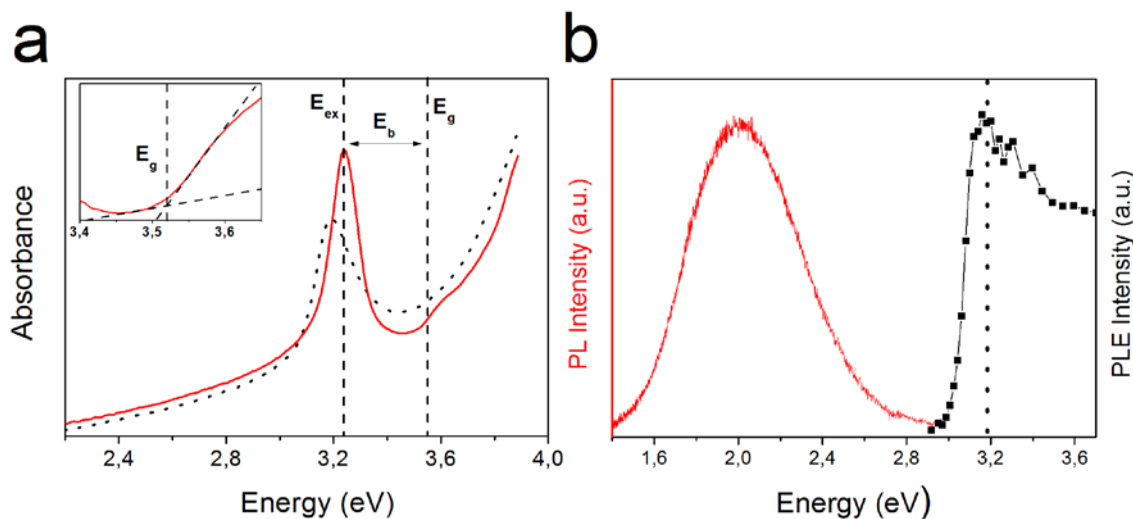


Figure 2. (a) Absorption spectra of (C₆H₁₁NH₃)₂PbBr₄ thin film measured at 300K (dotted line) and 12K (solid line). The inset shows the absorption spectrum at 12K around the band edge. E_{ex}, E_g and E_b represent the exciton energy, the energy gap, and the exciton binding energy, respectively. (b) Room temperature photoluminescence with E_{excit} = 3.815 eV (red) and photoluminescence excitation measured at 2.05 eV (black) spectra for (C₆H₁₁NH₃)₂PbBr₄ thin film. The dotted line indicates the position of the excitonic absorption peak at room temperature.

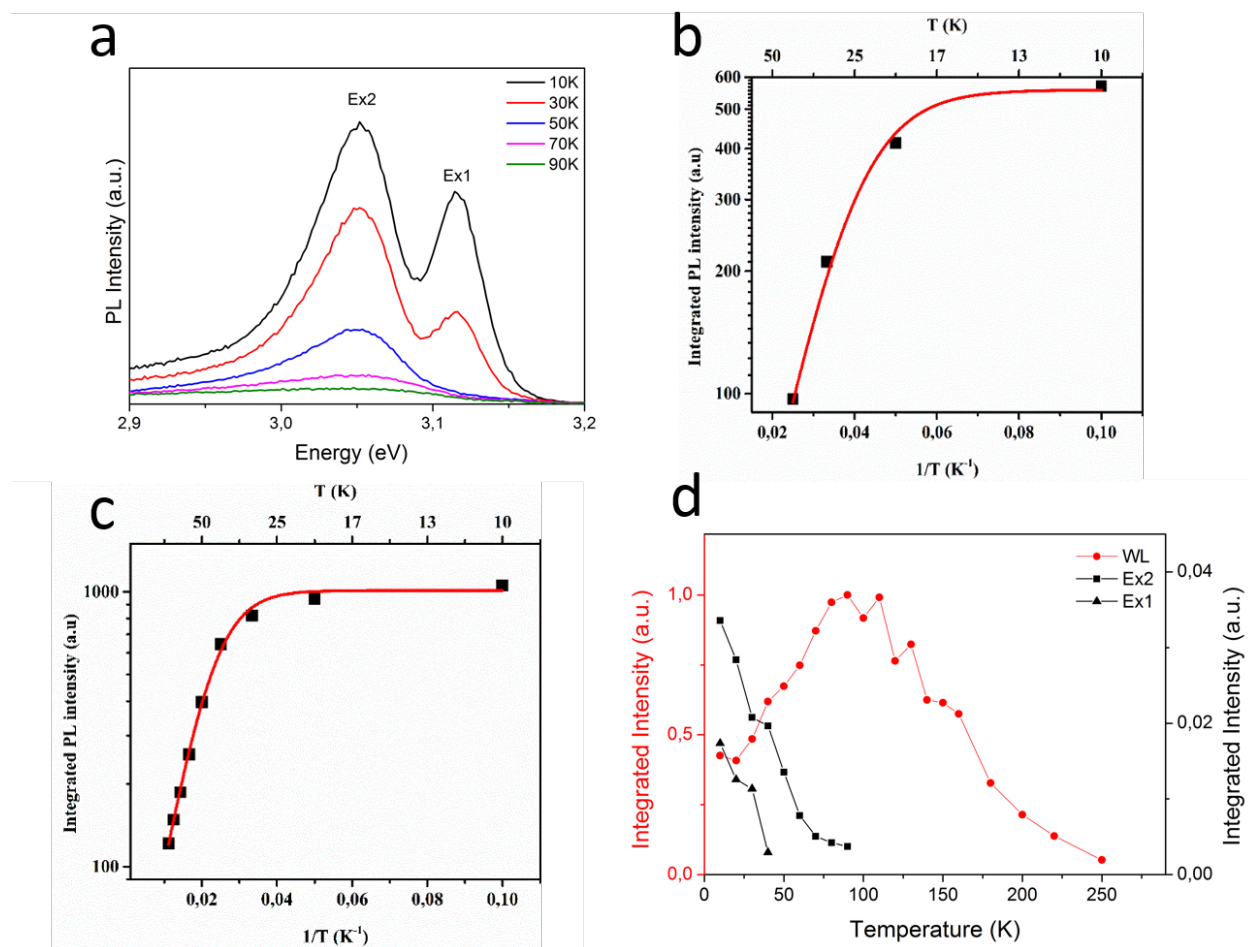


Figure 3. (a) PL spectra ($E_{\text{excit}} = 3.81$ eV) for temperatures ranging from 10K to 90K for Ex₁ and Ex₂. (b) Refinement of the thermal dependence of PL intensity of Ex₁ using Eq (1) with $I_0 = 558 \pm 20$, $a = 84.75 \pm 9.6$, and $E_a = 9.86 \pm 0.54$ meV and (c) Ex₂ with $I_0 = 1012.4 \pm 32$, $a = 55.845 \pm 4.93$, and $E_a = 14.93 \pm 0.86$ meV. (d) Thermal dependence of the integrated intensities of the Ex₁, Ex₂ and WL emissions peaks.

At low temperature, the high energy emission spectrum presents two additional sharp excitonic peaks, located at 3.11 eV (Ex₁) and 3.05 eV (Ex₂) (Figure 3a). There are no detectable shifts of these emissions as function of temperature. The peak at 3.11 eV is sharper than that at 3.05 eV with a FWHM of approximately 30 meV against 66 meV for Ex₂ and has a small stokes shift (less

1
2
3 than 10 meV). The Ex1 and Ex2 emission decrease quickly with temperature and are no more
4 detectable above 90K (Figure 3a). At higher temperature, the edge emission seems to disappear in
5 the background of the White Light (WL) emission. The coexistence of free and bound excitons is
6 often observed in hybrid perovskites.²⁹ Excitons could be trapped by weak potential of lattice
7 imperfections, such as defects, or structural disorder in general. Trapped excitons present a Stokes
8 shift due to this potential minima which decreases at higher the temperature and eventually
9 disappear when the thermal energy exceeds the trapping potential. Therefore, we could consider
10 Ex1 and Ex2 as free excitonic emission and shallow bound exciton respectively. We described the
11 quenching of Ex1 and Ex2 emission as due to a competition with a non-radiative channel as
12 described by the familiar law:³⁰

$$I = \frac{I_0}{1+a\exp\left(-\frac{E_a}{k_B T}\right)} \quad (1)$$

13 where I_0 is the zero-temperature PL intensity, k_B is the Boltzmann constant, a is the ratio
14 between the radiative and the non-radiative decay rates, and E_a is the activation energy. The best-
15 refinement gives: $E_a=9.86 \pm 0.54$ meV and $E_a=14.93 \pm 0.86$ meV for Ex1 and Ex2 respectively
16 (Figures 3b and 3c). The exciton binding energy could be deduced from low temperature
17 absorption spectroscopy. Figure 2b shows the absorption spectrum of our film measured at 12K.
18 The step-like structure at 3.5 eV correspond to the energy gap of the perovskite. An exciton binding
19 energy of 280 meV is deduced from the difference between the excitonic peak and the band gap
20 energies. This result is in good agreement with literature of PbBr_4 layered perovskites, where
21 reported binding energies are in the range of several hundred of meV: 200 to 300 meV for
22 $(\text{C}_n\text{H}_{2n+1}\text{NH}_3)_2\text{PbBr}_4$ ($n=4, 5, 7, 12$)²⁵ and 200 meV for $(\text{C}_6\text{H}_5\text{C}_2\text{H}_4\text{NH}_3)_2\text{PbBr}_4$ ²⁹, for example.
23 Consequently, the quenching of excitonic luminescence at low temperature could not correspond
24 to the exciton dissociation.

Now, we focus on the non-monotonous thermal behavior of the broad WL emission. The intensity of the WL emission excited at 3.815 eV increases with temperature, reaches a maximum at 100 K (Figure 3d) and then decreases and vanishes at ~ 250 K. Above 100 K, the PL intensity decreases on heating as $\exp(E/k_B T)$ with $E = 83 \pm 3.7$ meV. The increase of the PL intensity between 20 K and 100 K seems to be correlated with the decrease of the Ex1 and Ex2 peaks (Figure 3d). Therefore, our results strongly suggest that the quenching of the Ex1 and Ex2 in $(\text{C}_6\text{H}_{11}\text{NH}_3)_2\text{PbBr}_4$ could be attributed to the competition in the recombination process with the WL band.

A detailed inspection of the WL band shape shows a complex thermal evolution (Figure 4a). Indeed, the PL enhancement between 20 K and 100 K is accompanied by a narrowing of the emission and a red shift of the peak position of approximately 150 meV (Figure 4b and Figure 4c).

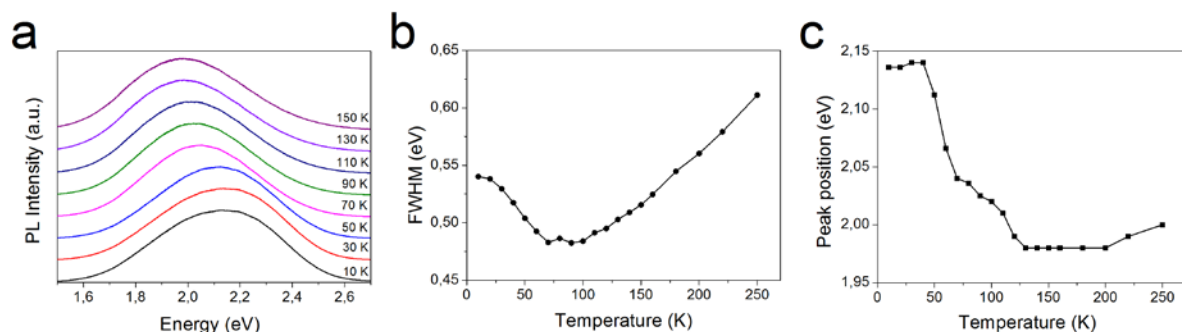


Figure 4. (a) Emission spectra between 10K and 150K. (Thermal evolution of the (b) FWHM and (c) peak position of the WL band under 3.815 eV excitation.

1
2
3 Hybrid organic-inorganic perovskites are known to present phase transitions, generally linked to
4 the organic layer of the material.^{31–33} These phase transitions could have an important impact on
5 the optical properties and in particular could results in band gap switching in 2D and 3D
6 HOP.^{10,34,35}
7
8
9
10

11 We have investigated the possible existence of a phase transition in $(\text{C}_6\text{H}_{11}\text{NH}_3)_2[\text{PbBr}_4]$ at low
12 temperature, which could be at the origin of the specific thermal behavior the WL emission.
13
14
15

16 Single crystal x-ray diffraction experiments were carried out at 20K, 50K, and 90K to detect the
17 presence of a possible structural phase transition in the [20-100K] temperature range. The details
18 on the data collection and structural refinement are summarized Table 2.
19
20
21
22
23

24 From 20K to 90K, the unit cell parameters do not show any significant features, besides usual
25 thermal expansion effects, the unit cell volume expanding regularly from 1940.3(1) Å³ to
26 1955.9(5) Å³. No space group change was detected, the three structures were determined in the
27 Cmc2₁ space group, in agreement with identical to the structure reported at 173K by Billing and
28 Lemmerer.³⁶ As shown in figure S1, the corresponding diffraction pattern do not exhibit any
29 evidence for a structural phase transition with change of unit cell constants, no superstructure
30 reflections were detected neither. By comparison with the results reported by Billing and
31 Lemmerer, only gradual evolution of the structural parameters are observed (see Table S1 in SI),
32 the inorganic layer do not undergo any abrupt distortion. In addition, the ammonium cation do not
33 exhibit any specific ordering, change of conformation, or change in N-H...Br hydrogen bond
34 network. Calorimetry measurements are also very important to assess the existence of a phase
35 transition.^{31–33}
36
37
38
39
40
41
42
43
44
45
46
47
48
49
50
51
52
53
54
55
56
57
58
59
60

Table 2. Low temperature crystallographic data

Temperature / K	20	50	90
Chemical formula	C ₁₂ H ₂₈ Br ₄ N ₂ Pb	C ₁₂ H ₂₈ Br ₄ N ₂ Pb	C ₁₂ H ₂₈ Br ₄ N ₂ Pb
Formula weight	727.19	727.19	727.19
Crystal system	Orthorhombic	Orthorhombic	Orthorhombic
Space group	Cmc2 ₁	Cmc2 ₁	Cmc2 ₁
a/Å	27.4995(10)	27.6108(12)	27.6460(16)
b/Å	8.6281(3)	8.6324(4)	8.637(2)
c/Å	8.1775(3)	8.1958(4)	8.1913(10)
Volume/Å ³	1940.26(12)	1953.45(16)	1955.9(5)
Z	4	4	4
ρ _{calc} g/cm ³	2.489	2.473	2.470
μ/mm ⁻¹	16.924	16.810	16.789
F(000)	1344	1344	1344
Crystal size/mm ³	0.216 × 0.342 × 0.058	0.216 × 0.342 × 0.058	0.223*0.315*0.042
Radiation	MoKα (λ = 0.71073)	MoKα (λ = 0.71073)	MoKα (λ = 0.71073)
2Θ range /°	3.512 to 28.280	2.951 to 28.278	2.947 to 28.274
hkl range	-36/27, -11/9, -9/10	-36/36, -11/11, - 10/10	-36/36, -11/11, - 10/10
collected reflections	5592	9574	9694
Independent reflections	2163 [R _{int} = 0.055]	2477 [R _{int} = 0.029]	2232 [R _{int} = 0.032]
parameters/restraints	80/14	80/8	80/8
^a Final R indexes	R ₁ = 0.036, wR ₂ = 0.082	R ₁ = 0.025, wR ₂ = 0.053	R ₁ = 0.032, wR ₂ = 0.078
^b Goodness-of-fit on F ²	1.097	1.044	1.138
Largest diff. peak/hole / e ⁻ Å ⁻³	1.67/-1.26	0.70/-1.25	1.09/-1.08

^aR₁ = Σ(|Fo-Fc|/Fo) [I ≥ 2σ (I)] and wR₂ = [Σ((ω(Fo²-Fc²))²/(ω(Fo²))²)]^{1/2} [all data].

^bG.O.F = [(Σ(ω(Fo²-Fc²))²/(Nobs-Nvar)]^{1/2}

The thermal dependence of the heat capacity (Figure 5) does not indicate the presence of any visible anomaly. Although these results do not allow to definitely exclude the existence of small rearrangements and/or smooth second order phase transitions, they clearly preclude the existence

of any first-order phase transition at low temperature. In particular, in the temperature interval 10-100K, where the thermal dependence of the PL showed the most significant variation, the heat capacity increases continuously following the usual trends of heat capacity of solids due to lattice phonons.

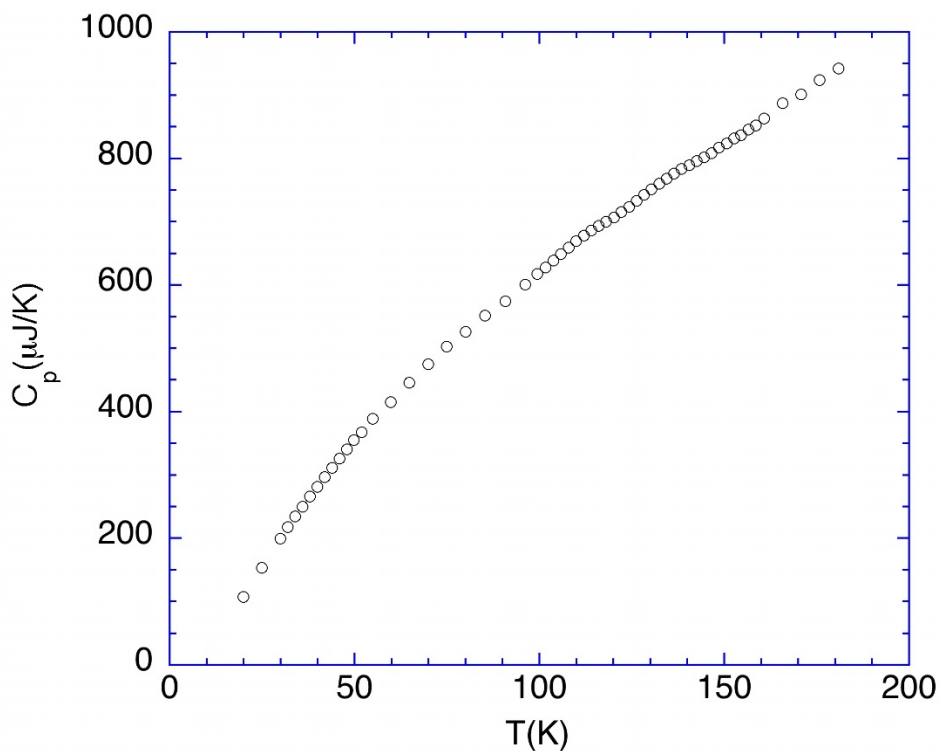


Figure 5: thermal dependence of the heat capacity of $(\text{C}_6\text{H}_{11}\text{NH}_3)\text{PbBr}_4$ showing a continuous behavior excluding the existence of a first order phase transition or a sharp second-order phase transition.

Based on the present crystallographic analysis and calorimetry measurements, the unusual thermal behavior of the PL WL emission could not be explained by the existence of a phase transition.

1
2
3 Another hypothesis is that the emission is in reality composed of different bands. To clarify this
4 point, we performed Time-Resolved Photoluminescence (TRPL) measurements as function of
5 temperature. Photoluminescence spectra at different delay show three distinct bands with maxima
6 at 2.05 eV, 2.29 eV and 2.5 eV respectively (Figure 6). The narrow peak at 2.43 eV at 10K is due
7 to an unknown impurity of the substrate. The 2.5 eV band is short-lived and disappears on a few
8 nanoseconds time scale. The Steady State Photoluminescence (SSPL) spectra (Figure 6) attests
9 that its contribution to the overall emission is weak compared to the two other bands. The already
10 presented complex thermal evolution of the WL band between 10K and 100K could be explained
11 by the thermal behavior of the 2.05 eV (WL1) and 2.29 eV bands (WL2). First, we do not detect
12 any measurable shift of these two bands as function of temperature. However, at 10K, the WL2
13 emission is more intense than WL1 and the overall emission maximum is at 2.22 eV. When the
14 temperature is raised, the WL1 emission increases relatively to the other band and the steady state
15 spectra progressively redshift to 2.15 eV at 100K.

16
17
18
19
20
21
22
23
24
25
26
27
28
29
30
31
32
33
34 Due to the important overlapping of the two emissions and the similarity of their decay
35 timescale, the exact shape and the specific lifetime of each band could not be properly separated.
36 Both luminescence decays of WL1 and WL2 exhibited a fast component (Figure 7a), not resolved
37 with our set-up, and a slow exponential tail. The best fit of this “slow” component was obtained
38 using a sum of two exponentials with time constant τ_1 and τ_2 . The WL2 emission is dominant just
39 after the excitation, at any temperature (Figure 6) due to its fast component. The slow luminescence
40 decay in the high energy side of the WL emission, where WL2 is predominant, is also faster than
41 in the low energy side (Figure 7b). To study the thermal evolution of this slow component, we
42 measured the luminescence decay of the WL emission, at the energy of its maximum. The
43 temperature-dependences of the decay times, τ_1 and τ_2 , were derived using the forthcoming
44
45
46
47
48
49
50
51
52
53
54
55
56
57
58
59
60

equation (2). The results, summarized in Figure 8, indicate that both constants undergo a significant decrease in the 10K-100K range.

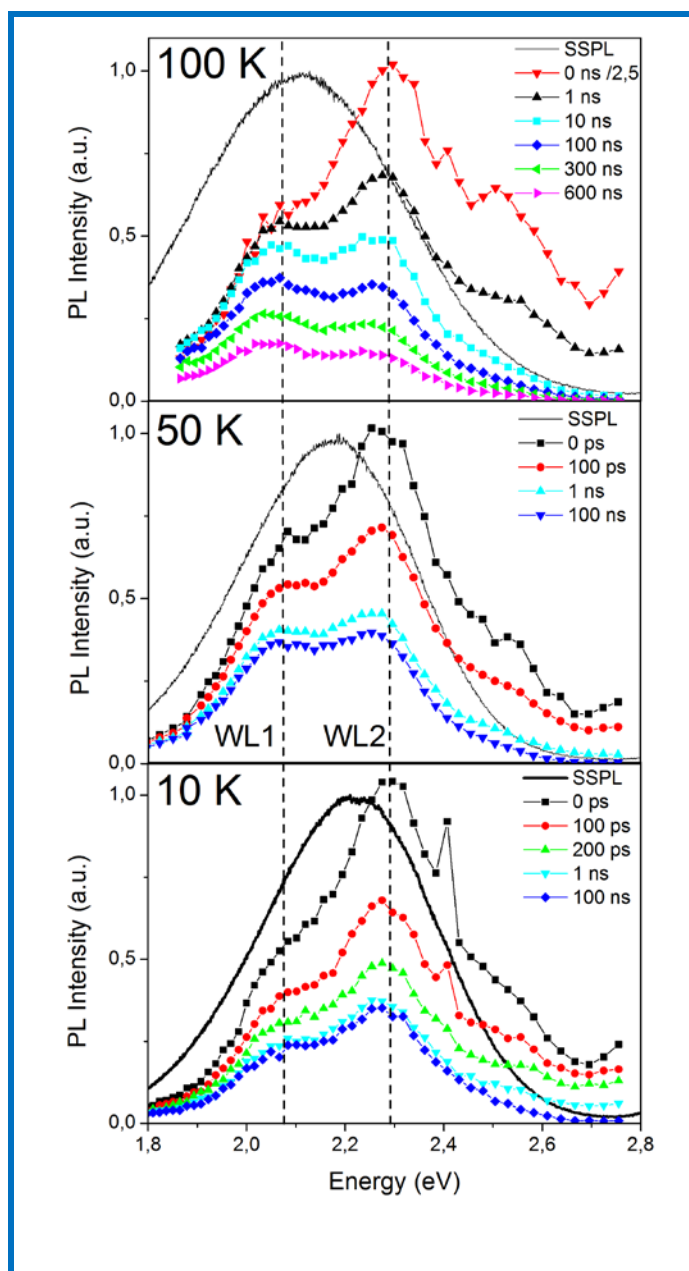


Figure 6. Steady-State and Time-Resolved photoluminescence spectra after excitation at 3.1 eV, at a temperature of 10K, 50K and 100K. Dashed lines indicate the position of the WL1 and WL2 band.

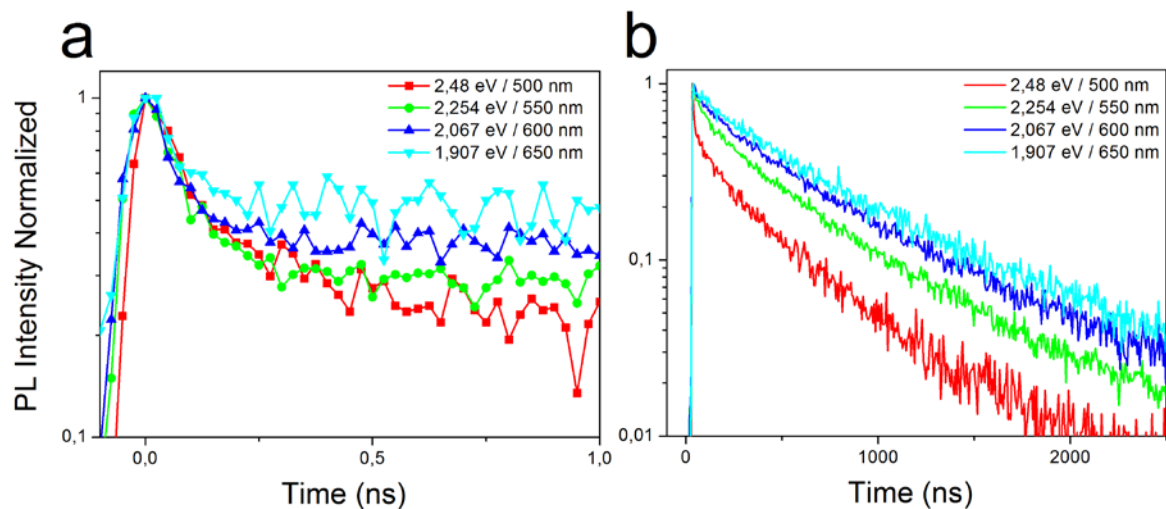


Figure 7. Normalized luminescence decay after excitation at 3.1 eV at 100K at different energies, on 1 ns (a) and 2500 ns time scales (b).

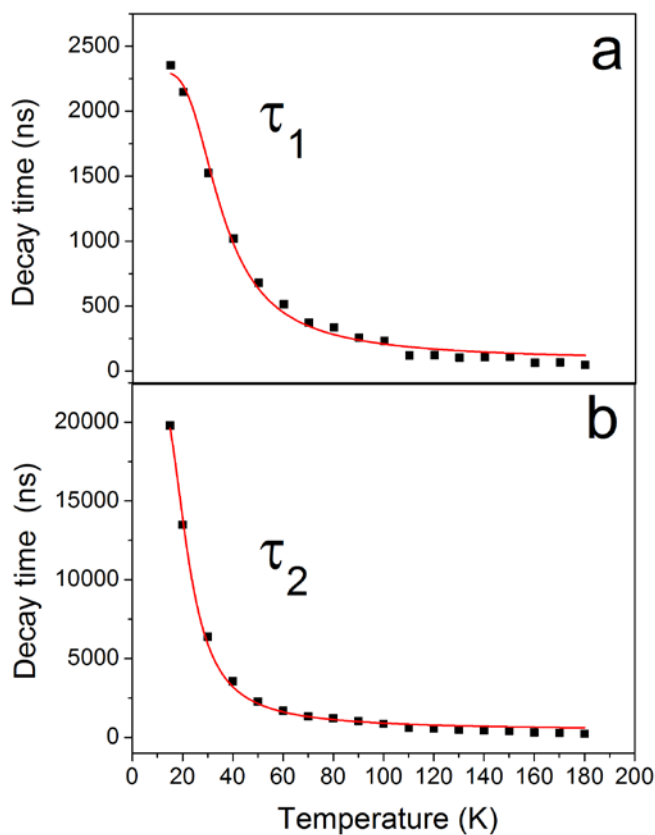
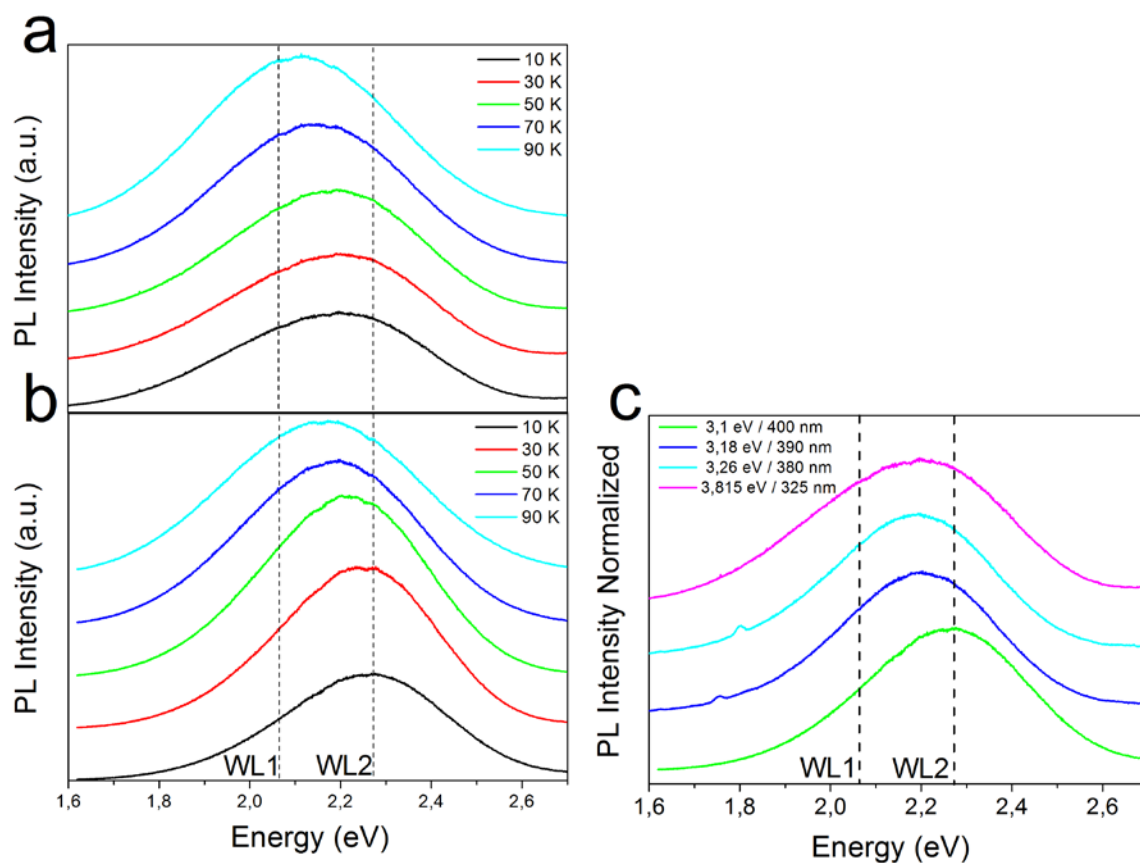


Figure 8. Temperature variation of the decay time constants obtained from the fit of the slow component with the sum of two exponentials. The experimental data are fitted with Equation 2

(red line) with (a) $E_1 = 11.5$ meV, $\tau_0 = 2295$ ns, $\nu = 0,017$ ns and (b) $E_2 = 7.9$ meV, $\tau_0 = 22075$ ns and $\nu = 0,027$ ns.

The weight of the two bands in the overall emission depends of the temperature but also, and more surprisingly, of the excitation energy, especially at low temperature. WL emission excited at 3.815 eV (325 nm) (Figure 9a) is clearly red-shifted and broader than the emission excited at 3.1 eV (400 nm) (Figure 9b). We infer that WL1 band is more effectively excited when we use 3.815 eV excitation. Note that at 3.1 eV, we excite the edge of the excitonic absorption while the 3.815 eV excitation is in the energy continuum of the semiconductor. As we raise the temperature, the WL1 emission increases relatively to WL2, as previously stated, and the difference between the overall WL emission excited at 3.1 eV and 3.815 eV becomes less significant.



1
2
3 **Figure 9.** WL emission shape as a function of temperature and with excitation at (a) 3.851 eV (a)
4 and (b) 3.1 eV. (c) WL emission spectra for different excitation energies at 10K. Spectra are offset
5 for clarity. Dashed lines indicate the position of the WL1 and WL2 band.
6
7
8
9

10
11 To go further, we studied the shape of the WL emission at different excitation energies at the
12 same temperature (Figure 9c). As we increase the excitation energy, we clearly observe that the
13 emission redshifts and broaden. This result corroborate the hypothesis that the WL2 emission is
14 excited preferentially at high excitation energy. By comparing Figure 9a with Figure 9c, the
15 evolution of the shape of the emission as we raised the excitation energy seems close to the one
16 observed when we increase the temperature from 10K to 100K, for the same excitation energy.
17
18
19
20
21
22
23
24
25
26

27
28 We discuss now the possible physical origin of this WL emission. We could consider two
29 hypothesis. First, broad PL with important Stokes shift could result of the recombination of
30 carriers localized at defects or impurities.^{27,37} A strong coupling between the electronic states of
31 the imperfection and the phonons of the crystal through the electron-phonon interaction could give
32 rise to vibronics bands. In contrast with interband transition, the continuous spectral band of the
33 imperfection come from the coupling of the discrete electronic states to the phonons. The excited
34 state is shifted compared to the ground state by the electron-phonon interaction, measured by the
35 Huang-Rhys factor. This shift is responsible for the energy difference between the absorption and
36 the emission of the defect (Stokes shift), and also explains the width of the emission (Figure 10a).
37
38 In fact, the carriers relax to the zero vibrational level of the ground state by emitting a photon and
39 several phonons. Deep center defects lead to broad, Gaussian shaped emission with a large Stokes
40 shift as for the case of the Yellow Band in GaN.²⁷
41
42
43
44
45
46
47
48
49
50
51
52
53
54
55
56
57
58
59
60

1
2
3 Second, self-trapping of excitons or electrons/holes gives also rise to broad-bands, Gaussian
4 shaped and strongly Stoke-shifted luminescence, which have been studied in alkali, ammonium
5 and lead halide.³⁸⁻⁴¹ Due to strong lattice coupling, charge carriers could be trapped in their own
6 lattice distortion. In lead bromide, the recombination of self-trapped excitons and also of self-
7 trapped holes with self-trapped electrons has been well studied.⁴² The coexistence of free and self-
8 trapped excitons has also been observed in alkali halide.^{41,43} The mechanism of this coexistence
9 could be described in a configuration coordinate diagram (Figure 10b). The conversion of a free
10 exciton into a self-trapped exciton requires to overcome a potential barrier by thermal activation
11 or tunneling effect.⁴⁰ In some cases, excitons could also relax directly to the self-trapped state
12 without passing through the bottom of the free-exciton band³⁸ (Figure 10b). The tunneling and the
13 direct path should be relatively independent of temperature. The energy barrier E_B is linked to the
14 elastic deformation required for the exciton localization. The presence of permanent trap state
15 could also help to localize the carrier when the electron-phonon coupling is not sufficient. In this
16 case, an energy barrier could be observed between the defect and the self-trapped state. This
17 situation is referred as extrinsic self-trapping⁴⁴.
18
19
20
21
22
23
24
25
26
27
28
29
30
31
32
33
34
35
36
37
38
39
40
41
42
43
44
45
46
47
48
49
50
51
52
53
54
55
56
57
58
59
60

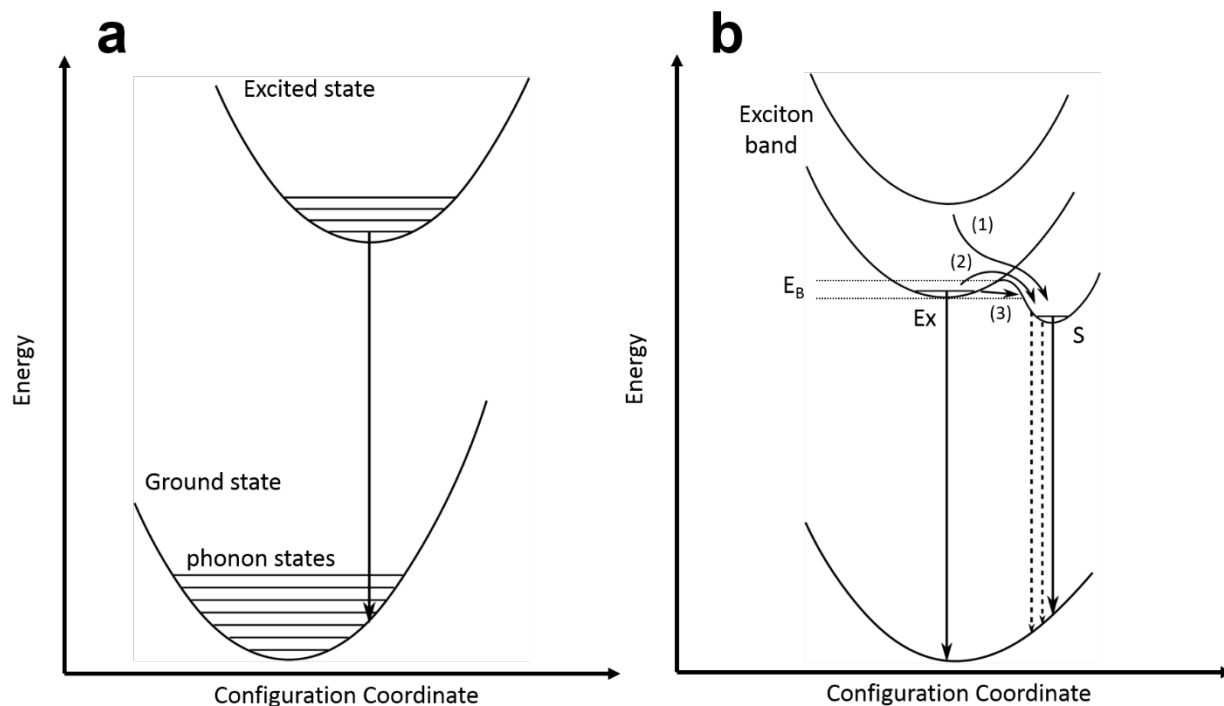
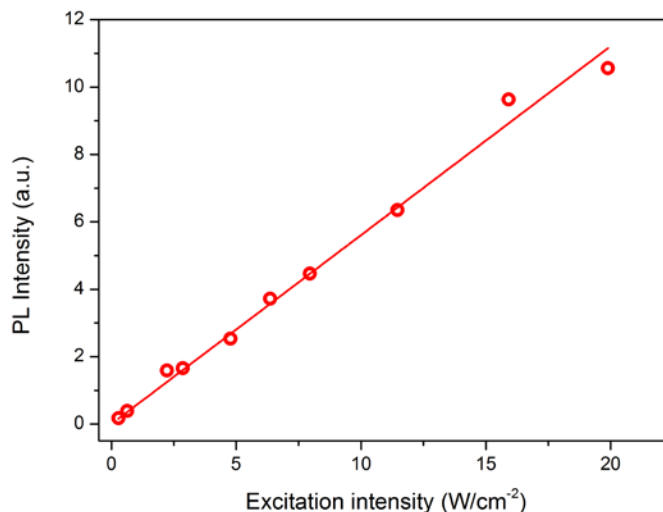


Figure 10: (a) An example of Configuration Coordinate diagram for a deep-level defect. (b) CC diagram illustrating the coexistence of free and self-trapping excitons. The letters Ex and S show the free and self-trapped state respectively. Three distinct path toward self-trapping are represented: direct relaxation (1) thermal overcoming of the barrier (2) and tunneling (3).

We now consider the consistency of our results in the framework of these two hypothesis. First, permanent defect concentration and recombination lifetime are finite, thus their PL could be saturated at high excitation power.²⁷ However, the intensity of the WL luminescence presents a linear dependence with intensity up to 20 W/cm^2 , as shown in Figure 11; the absence of saturation is in good agreement with the results of Dohner and al. on (N-MEDA)PbBr₄ and (EDBE)PbBr₄^{21,22}. Above 20 W/cm^2 of excitation intensity, the photo-degradation of the films unfortunately becomes non-negligible. The self-trapped carriers could be considered as transient

1
2
3 defect states and thus, the absence of the saturation of the PL intensity with intensity is consistent
4
5
6 with this hypothesis.
7
8
9



10
11
12
13
14
15
16
17
18
19
20
21
22
23
24
25
26
27
28
29 **Figure 11.** PL intensity of the WL band vs excitation power density
30
31

32 Concerning the thermal behavior of the emission, we observe that, below 20K, the WL emission
33 is nearly constant and then in the 20 K-100 K range, it increases at the expense of the Ex1 and Ex2
34 emission. In classical semiconductors like GaN, the increase of defect related PL as the excitonic
35 emission quenches is generally explained by the dissociation of the exciton and the redistribution
36 of electrons/holes toward the defect. But in the case of (C₆H₁₁NH₃)PbBr₄, the binding energy is
37 important and we have discarded the possibility that the quenching of Ex1 and Ex2 at low
38 temperature correspond to the free exciton dissociation. Besides, the WL emission decreases
39 drastically at room temperature and should not be able to compete efficiently in the recombination
40 process with the free excitonic emission. Consequently, one would expect to detect the free
41 excitonic emission at room temperature. In the framework of self-trapping, the existence of an
42 energy barrier in the adiabatic potential energy surface explains these unusual observations in a
43
44
45
46
47
48
49
50
51
52
53
54
55
56
57
58
59
60

1
2
3 direct manner by the thermal overcoming of the barrier (Figure 10b). The quenching of the edge
4 emission with an energy of 10-15 meV gives an order of magnitude of the energy barrier. This
5 value is close to those reported for alkali-halide (eg KI : 14 meV-33meV⁴⁵, NaI 17 meV⁴⁶).
6
7

8
9
10 In this hypothesis, the thermal evolution of the luminescence decay rate should be dominated by
11 the thermal overcoming of the energy barrier process. The probability $1/\tau_{th} = \nu e^{-E/k_B T}$ for self-
12 trapping by thermal transition includes the energy barrier, E (k_B is the Boltzmann constant) and
13 the rate constant ν ^{46,47}. Hence, luminescence decay constants of figure 8 have been fitted with the
14 following law:
15
16
17
18
19
20
21

$$22 \quad 1/\tau = 1/\tau_0 + \nu e^{-E/k_B T} \quad (2)$$

23
24
25
26
27
28 with $1/\tau_0 = 1/\tau_r + 1/\tau_t$, where $1/\tau_t$ is the tunneling rate and $1/\tau_r$ is the transition probability
29 by radiative recombination from the S state (Figure 10b). We have considered $1/\tau_0$ as relatively
30 independent of temperature compared to $1/\tau_{th}$. The results clearly indicate that the luminescence
31 decay constants decrease exponentially with temperature as expected. Within this model, two
32 energies were derived: $E_2 = 7.9 \pm 0.3 \text{ meV}$ and $E_1 = 11.5 \pm 0.6 \text{ meV}$ from the thermal
33 evolution of τ_2 and τ_1 . These values are close to those measured for the quenching of the free
34 excitonic emission. The precise assignation of these two distinct energies is not straightforward,
35 partly because we could not separate the WL1 and WL2 contributions.
36
37
38
39
40
41
42
43
44
45
46
47

48 Finally, we remark previously that both raising the temperature or the excitation energy result in
49 a relative increase the WL1 emission. This very unusual behavior could be explained again in the
50 framework of self-trapping. As stated previously, excitons created at high energy have the
51 possibility to relax directly into the self-trapped state. Raising the excitation energy increases the
52
53
54
55
56
57
58
59
60

1
2
3 direct relaxation path efficiency, while raising the temperature allow the thermal overcoming of
4 the barrier (Figure 10b).
5
6

7
8 All these experimental observations find a direct and consistent explanation with the hypothesis
9 of self-trapped carriers. The WL1 and WL2 bands could correspond to excitons self-trapped on
10 two different sites, with two distinct energy barriers. Another possibility is that the WL2 emission
11 corresponds to a permanent trap state separated by an energy barrier from a self-trapped state (WL1
12 band), as described in the case of extrinsic self-trapping. Further investigation are needed and
13 particularly calculations of the electronic structure will be very helpful.
14
15
16
17
18
19
20
21
22
23

24 IV. CONCLUSIONS

25
26 We described the optical properties of white light emission under UV irradiation in
27 $(\text{C}_6\text{H}_{11}\text{NH}_3)_2\text{PbBr}_4$ thin films. The WL emission coexists at low temperature with an excitonic
28 edge emission. Low temperature optical absorption allows to estimate the free exciton binding
29 energy to 280 meV. However, the excitonic edge luminescence disappeared when the temperature
30 is raised from 10K to 90K whereas the WL emission increases to reach a maximum. Heat capacity
31 measurements and X-ray diffraction investigations did not show the presence of any first order
32 phase transition at the origin of this non-monotonous thermal behavior. Time-Resolved
33 photoluminescence investigations show that the white luminescence decay time decreases
34 exponentially with temperature in the same temperature range. Time-Resolved absorption spectra
35 demonstrates that the WL emission is composed of mainly two bands. The weight of these two
36 bands in the overall emission changes with of the temperature and excitation energy. Overall, the
37 results find a straightforward explanation if we consider that the luminescence originates from
38
39
40
41
42
43
44
45
46
47
48
49
50
51
52
53
54
55
56
57
58
59
60

1
2
3 self-trapped states and the existence of an energy barrier against self-trapping of approximately 10
4
5 meV.
6
7
8
9

10 AUTHOR INFORMATION

13 Corresponding Authors

16 *Email: damien.garrot@uvsq.fr, kbo@physique.uvsq.fr

19 Notes

21 The authors declare no competing financial interests.
22
23
24

25 ACKNOWLEDGMENT

27 This work was supported by the PHC MAGHREB program N° N° 13MAG08&30255ZJ, the
28 "Agence Nationale de la Recherche" (ANR project BISTA-MAT: ANR-12-BS07-0030-01),
29 Spanish MINECO (through the grant MAT2013-44063-R), Université de Versailles Saint-
30 Quentin-En-Yvelines, CNRS, and Université de Sfax, which we deeply acknowledge.
31
32
33
34
35
36
37
38
39

40 REFERENCES

- 42 (1) Mitzi, D. B. Synthesis, structure, properties of organic-inorganic perovskites and related
43 materials. *Prog. Inorg. Chem., Vol 48* **1999**, *48*, 1–121.
- 44 (2) Papavassiliou, G.; Koutselas, I. Structural, optical and related properties of some natural
45 3-dimensional and lower-dimensional semiconductor systems. *Synth. Met.* **1995**, *71*,
46 1713–1714.
- 47 (3) Burschka, J.; Pellet, N.; Moon, S.-J.; Humphry-Baker, R.; Gao, P.; Nazeeruddin, M. K.;
48 Graetzel, M. Sequential deposition as a route high-performance perovskite sensitized
49 solar cells. *Nature* **2013**, *499*, 316-319.
- 50 (4) Kojima, A.; Teshima, K.; Shirai, Y.; Miyasaka, T. Organometal halide perovskites
51 visible-light sensitizers for photovoltaic cells. *J. Am. Chem. Soc.* **2009**, *131*, 6050-6051.
- 52 (5) Lee, M. M.; Teuscher, J.; Miyasaka, T.; Murakami, T. N.; Snaith, H. J. Efficient hybrid
53 solar cells based on meso-superstructured organometal halide perovskites. *Science* **2012**,
54 *338*, 643–647.
55
56
57
58
59
60

- 1
- 2
- 3
- 4 (6) Liu, M.; Johnston, M. B.; Snaith, H. J. Efficient planar heterojunction perovskite Solar
- 5 cells by vapour deposition. *Nature* **2013**, *501*, 395–398.
- 6 (7) Zhou, H.; Chen, Q.; Li, G.; Luo, S.; Song, T.; Duan, H.-S.; Hong, Z.; You, J.; Liu, Y.;
- 7 Yang, Y. Interface engineering of highly efficient perovskite solar cells. *Science* **2014**,
- 8 *345*, 542–546.
- 9 (8) Xing, G.; Mathews, N.; Lim, S. S.; Yantara, N.; Liu, X.; Sabba, D.; Gratzel, M.;
- 10 Mhaisalkar, S.; Sum, T. C. Low temperature solution-processed wavelength-tunable
- 11 perovskites for lasing. *Nat. Mater.* **2014**, *13*, 476–480.
- 12 (9) Calabrese, J.; Jones, N. L.; Harlow, R. L.; Herron, N.; Thorn, D. L.; Wang, Y. Preparation
- 13 and characterization of layered lead halide compounds. *J. Am. Chem. Soc.* **1991**, *113*,
- 14 *2328–2330*.
- 15 (10) Ishihara, T. Optical properties of PbI-based perovskite structures. *J. Lumin.* **1994**, *60-1*,
- 16 *269–274*.
- 17 (11) Gauthron, K.; Lauret, J. S.; Doyennette, L.; Lanty, G.; Al Choueiry, A.; Zhang, S. J.;
- 18 Brehier, A.; Largeau, L.; Mauguin, O.; Bloch, J.; et al. Optical spectroscopy of two-
- 19 dimensional layered (C₆H₅C₂H₄-NH₃)₂-PbI₄ perovskite. *Opt. Express* **2010**, *18*, 5912–
- 20 5919.
- 21 (12) Ishihara, T.; Takahashi, J.; Goto, T. Optical properties due to electronic transitions in 2-
- 22 dimensional semiconductors (C_nH_{2n+1}NH₃)₂PbI₄. *Phys Rev B* **1990**, *42*, 11099–11107.
- 23 (13) Era, M.; Morimoto, S.; Tsutsui, T.; Saito, S. Organic-inorganic heterostructure
- 24 electroluminescent device using a layered perovskite semiconductor
- 25 (C₆H₅C₂H₄NH₃)₂PbI₄. *Appl. Phys. Lett.* **1994**, *65*, 676–678.
- 26 (14) Hattori, T.; Taira, T.; Era, M.; Tsutsui, T.; Saito, S. Highly efficient electroluminescence
- 27 from a heterostructure device combined with emissive layered-perovskite and an electron-
- 28 transporting organic compound. *Chem. Phys. Lett.* **1996**, *254*, 103–108.
- 29 (15) Kagan, C. R.; Mitzi, D. B.; Dimitrakopoulos, C. D. Organic-inorganic hybrid materials as
- 30 semiconducting channels in thin film field effect transistors. *Science* **1999**, *286*, 945–947.
- 31 (16) Brehier, A.; Parashkov, R.; Lauret, J. S.; Deleporte, E. Strong exciton-photon coupling in
- 32 a microcavity containing layered perovskite semiconductors. *Appl. Phys. Lett.* **2006**, *89*,
- 33 *171110*.
- 34 (17) Lanty, G.; Zhang, S.; Lauret, J. S.; Deleporte, E.; Audebert, P.; Bouchoule, S.; Lafosse,
- 35 X.; Zuniga-Perez, J.; Semond, F.; Lagarde, D.; et al. Hybrid cavity polaritons in a ZnO-
- 36 perovskite microcavity. *Phys Rev B* **2011**, *84*, 195449.
- 37 (18) Braun, M.; Tuffentsammer, W.; Wachtel, H.; Wolf, H. C. Tailoring energy levels in lead
- 38 chloride based layered perovskites and energy transfer between the organic and inorganic
- 39 planes. *Chem. Phys. Lett.* **1999**, *303*, 157–164.
- 40 (19) Zhang, S. J.; Audebert, P.; Wei, Y.; Lauret, J. S.; Galmiche, L.; Deleporte, E. Synthesis
- 41 and optical properties of novel organic-inorganic hybrid UV (RNH₃)₂PbCl₄
- 42 semiconductors. *J. Mater. Chem.* **2011**, *21*, 466–474.
- 43 (20) Zhang, S. J.; Lanty, G.; Lauret, J. S.; Deleporte, E.; Audebert, P.; Galmiche, L. Synthesis
- 44 and optical properties of novel organic-inorganic hybrid nanolayer structure
- 45 semiconductors. *Acta Mater.* **2009**, *57*, 3301–3309.
- 46 (21) Dohner, E. R.; Hoke, E. T.; Karunadasa, H. I. Self-Assembly broadband white-light
- 47 emitters. *J. Am. Chem. Soc.* **2014**, *136*, 1718–1721.
- 48 (22) Dohner, E. R.; Jaffe, A.; R., B. L.; Karunadasa, H. I. Intrinsic white light emission in
- 49 layered hybrid perovskites. *J. Am. Chem. Soc.* **2014**, *136*, 13154–13157.
- 50
- 51
- 52
- 53
- 54
- 55
- 56
- 57
- 58
- 59
- 60

- 1
2
3
4
5
6
7
8
9
10
11
12
13
14
15
16
17
18
19
20
21
22
23
24
25
26
27
28
29
30
31
32
33
34
35
36
37
38
39
40
41
42
43
44
45
46
47
48
49
50
51
52
53
54
55
56
57
58
59
60
- (23) Sheldrick, G. M. A short History of SHELX. *Acta Crystallographica Section A* **2008**, *64*, 112–122.
- (24) CrysAlis CCD; CrysAlis RED, *version 171.37.31*, Oxford Diffraction, Wroclaw, Poland **2014**.
- (25) Kitazawa, N.; Aono, M.; Watanabe, Y. Excitons in organic-inorganic hybrid compounds $(C_nH_{2n+1}NH_3)_2PbBr_4$ ($n=4, 5, 712$). *Thin Solid Films* **2010**, *518*, 3199–3203.
- (26) Kitazawa, N.; Watanabe, Y. Optical properties of natural quantum-well compounds $(C_6H_5-C_nH_{2n}-NH_3)_2PbBr_4$ ($n=1-4$). *J. Phys. Chem. Solids* **2010**, *71*, 797–802.
- (27) Reshchikov, M.; Morkoc, H. Luminescence properties of defects in GaN. *J. Appl. Phys.* **2005**, *97*, 061301.
- (28) Tanaka, K.; Takahashi, T.; Kondo, T.; Umeda, K.; Ema, K.; Umebayashi, T.; Asai, K.; Uchida, K.; Miura, N. Electronic and excitonic structures of inorganic-organic perovskite-type quantum-well crystal $(C_4H_9NH_3)_2PbBr_4$. *Jpn. J. Appl. Phys., Part 1* **2005**, *44*, 5923–5932.
- (29) Kitazawa, N.; Aono, M.; Watanabe, Y. Temperature-dependent time-resolved photoluminescence of $(C_6H_5C_2H_4NH_3)_2PbX_4$ ($X = BrI$). *Mater. Chem. Phys.* **2012**, *134*, 875–880.
- (30) Jiang, D.; Jung, H.; Ploog, K. Temperature-dependence of photoluminescence from Gaas single and multiple quantum-well heterostructures grown by molecular-beam epitaxy. *J. Appl. Phys.* **1988**, *64*, 1371–1377.
- (31) Billing, D. G.; Lemmerer, A. Synthesis, characterization and phase transitions of the inorganic-organic layered perovskite-type hybrids $[(C_nH_{2n+1}NH_3)_2PbI_4]$ ($n=12, 14, 16$ and 18). *New J. Chem.* **2008**, *32*, 1736–1746.
- (32) Billing, D. G.; Lemmerer, A. Synthesis, characterization and phase transitions in the inorganic-organic layered perovskite-type hybrids $[(C_nH_{2n+1}NH_3)_2PbI_4]$, $n=4, 5$ and $6, n=4,5 6$. *Acta Crystallogr B* **2007**, *63*, 735–747.
- (33) Onoda-Yamamuro, N.; Matsuo, T.; Suga, H. Calorimetric and IR Spectroscopic Studies of Phase Transitions in Methylammonium Trihalogenoplumbates. *Journal of Physics and Chemistry of Solids* **1990**, *51*, 1383–1395.
- (34) Koubaa, M.; Dammak, T.; Garrot, D.; Castro, M.; Codjovi, E.; Mlayah, A.; Abid, Y.; Boukheddaden, K. Thermally-induced first-order phase transition in the $(FC_6H_4C_2H_4NH_3)_2[PbI_4]$ photoluminescent organic-inorganic material. *J. Appl. Phys.* **2012**, *111*, 053521.
- (35) Pradeesh, K.; Baumberg, J. J.; Prakash, G. V. Temperature-induced exciton switching in long alkyl chain based inorganic-organic hybrids. *J. Appl. Phys.* **2012**, *111*, 013511.
- (36) Billing, D. G.; Lemmerer, A. Inorganic-organic hybrid materials incorporating primary cyclic ammonium cations: The lead bromide and chloride series. *Crystengcomm* **2009**, *11*, 1549–1562.
- (37) McCluskey, M. D.; Jokela, S. J. Defects in ZnO. *J. Appl. Phys.* **2009**, *106*, 071101
- (38) Fugol, I. Excitons in rare gas crystals. *Adv Phys* **1978**, *27*, 1–87.
- (39) Plekhanov, V. Lead halides: Electronic properties applications. *Prog Mater Sci* **2004**, *49*, 787–886.
- (40) Toyozawa, Y. Self-trapping of an electron by the acoustical mode of lattice vibration.1. *Prog Theor Phys* **1961**, *26*, 29–44.
- (41) Williams, R.; Song, K. The self-trapped exciton. *J. Phys. Chem. Solids* **1990**, *51*, 679–716.

- 1
2
3 (42) Iwanaga, M.; Hayashi, T. Exciton-relaxation dynamics in lead halides. *J. Lumin.* **2003**, *102*,
4 663–668.
5
6 (43) Lushchik, A.; Kirm, M.; Lushchik, C.; Martinson, I.; Zimmerer, G. Luminescence of free
7 and self-trapped excitons in wide-gap oxides. *J. Lumin.* **2000**, *87-89*, 232–234.
8
9 (44) Stoneham, A. M.; Gavartin, J.; Shluger, A. L.; Kimmel, A. V.; Ramo, D. M.; Ronnow, H.
10 M.; Aeppli, G.; Renner, C. Trapping, self-trapping and the polaron family. *J. Phys.*
11 *Condens. Matter* **2007**, *19*, 255208
12
13 (45) Vankhien, T.; Nouailhat, A. The Free Exciton In Ki_2 . Coexistence With The Self-Trapped
14 Exciton. *J. Phys. Soc. Jpn.* **1981**, *50*, 127–128.
15
16 (46) Nishimura, H.; Ohhigashi, C.; Tanaka, Y.; Tomura, M. Resonance luminescence lines of
17 of free excitons in alkali iodide single-crystals. *J. Phys. Soc. Jpn.* **1977**, *43*, 157–163.
18
19 (47) Matsui, A.; Mizuno, K.; Tamai, N.; Yamazaki, I. Transient free-exciton luminescence and
20 exciton-lattice interaction in pyrene crystals. *Chem. Phys.* **1987**, *113*, 111–117.
21
22
23
24
25
26
27
28
29
30
31
32
33

TOC GRAPHICS

